ICDFP8–EG–178
Eighth International Congress of Fluid Dynamics & Propulsion
December 14 -17 2006, Sharm El-Shiekh, Egypt

Steady and Pulsed Fluidic Actuation for Cavity Acoustics Control

K. Das*, A. Hamed and D. Basu***

***Research Engineer**
Center for Nuclear Waste Regulatory Analyses,
Southwest Research Institute,
San Antonio, Texas 78238

****Professor and Head**
Department of Aerospace Engineering and Engineering Mechanics
University of Cincinnati
Cincinnati, OH 45221-0070

ABSTRACT

A numerical study is conducted to investigate fluidic actuation for acoustic suppression in transonic flow over an open cavity. Numerical results are obtained for the unsteady three-dimensional Navier Stokes equations for different steady and pulsed mass injection rates upstream of the cavity. Detached eddy simulations (DES) are used to obtain computational results are presented for the unsteady flow and acoustic fields, which are compared for different steady and pulsed mass flow ratios. Computational results are presented for the SPL spectra to highlight the effectiveness of actuation on tone attenuation at the dominant frequencies. The computed sound pressure level (SPL) spectra are compared with experimental results and with results from large eddy simulations (LES) for pulsed and no injection. Additional results are presented for the Mach number and turbulent kinetic energy to characterize the change in the unsteady flow field with steady and pulsed injection.

INTRODUCTION

Several techniques have been investigated for acoustic suppression of flow over open cavities [1-11]. In general passive suppression techniques like fences [1] and spoilers [2,3] had achieved limited success under high speed flow conditions. An experimental study by Stanek et al. [4] of rods, spoilers and rods modified with circular end-caps linked high frequency rod shedding to acoustic suppression. Active control techniques on the other hand have been effectively used for noise reduction over a wide range of operating conditions. These techniques include oscillating flaps [5], upstream steady mass injection [6], harmonic blowing [7,8], piezoelectric actuators [9,10] and powered resonance tubes [11].

Shaw and Northcraft [8] investigated the effect of steady mass injection upstream of the cavity at subsonic Mach numbers and determined that SPL decreases with increased mass injection. Stanek et al. [12] conducted a thorough experimental study in subsonic and supersonic cavity flow fields using four high-frequency actuators (piezo-ceramic wedge, rod in cross-flow, passive resonance tube, powered resonance tube) and a low frequency actuator (saw-toothed spoiler). They reported that the high frequency powered resonance tube was most effective in reducing the peak tones at the dominant frequencies. In a subsequent study, Stanek et al. [13] compared the effect of steady and pulsed mass actuation and observed that a substantial amount of suppression can be attributed to the steady injection. They introduced the notion of superposition of steady effect and high frequency effect and proposed that high frequency forcing stabilizes the flow rather than drain energy out of the large scales as suggested by Glezer et al. [14]. Ukeiley et al. [15] investigated a powered whistle in supersonic flow and steady mass blowing of nitrogen helium and hot air in subsonic flow, and observed that helium injection was most effective in decimating the Rossiter tones. Zhuang et al. [16] conducted experiments in supersonic cavity flow control using supersonic microjets at the leading edge, and reported a 10dB reduction in the overall SPL and 20 dB reductions at tonal frequencies.

Fewer numerical studies have been conducted for cavity flow control. Cain et al. [17,18] performed 2D URANS simulations of harmonic mass injection in subsonic cavity flows and concluded that the mean mass flow plays a more important role than the actuation frequency in noise suppression.

Arunajatesan et al. [20,21] performed 2D RANS and 3D hybrid RANS/LES simulations of subsonic flow over cavity using a thin rod as suppression device.

They showed that the 2D simulations exhibit a wake mode behavior, which is not consistent with experimental observation. The study presented auto and cross-correlation functions, two-point correlation tensors and turbulent and kinetic energy budgets from the 3D simulations in an attempt to explain the control mechanism. Rizzetta et al. [19] performed large eddy simulations (LES) of high frequency mass pulsing in supersonic cavity flows and characterized the resulting suppression. Computational studies of the current authors based on direct numerical simulations [22] and detached eddy simulations [23,24] indicated a noticeable increase in pressure fluctuation amplitude with Mach number [22], and an increase in the sound pressure level (SPL) with the flow Reynolds number [23,24]. Preliminary studies on steady blowing by the current authors indicated a 7.5–10% reduction in RMS pressure load across the cavity floor using a 6–9% injection mass ratio [25, 26].

In the present work, numerical simulations are carried for steady blowing and high frequency mass actuation to gain an understanding of acoustic control in a transonic cavity at different mass injection ratios and forcing frequencies. Computational results for Sound Pressure Level (SPL) spectra are compared with experimental data and LES results for unsteady actuation. Comparisons of predicted SPL spectra for the base line and the controlled cases show a reduction in SPL peak amplitude at the dominant frequencies, which are greater and are accompanied by a reduction in broadband noise for pulsed injection. The presented results indicate that reduced turbulent kinetic energy in the shear layer due to pulsed injection is associated with the noise reduction is associated with

METHODOLOGY

The unsteady, three-dimensional compressible Navier-Stokes equations in strong conservation-law form are solved numerically using implicit approximate-factorization Beam-Warming scheme [27]. Newton subiterations are employed to improve temporal accuracy and stability of the algorithm. Details of the numerical algorithm in the parallel version of the time accurate three-dimensional solver FDL3DI, originally developed at AFRL, can be found in reference 28. The solver was been extensively validated and proved to be efficient for a wide range of high speed and low speed; steady and unsteady problems [19,29,30]. For the present research, the two-equation k-ε based DES model [31-33] was implemented in the solver to conduct the unsteady high-speed flow simulations. The DES method was demonstrated to provide the required dynamic range resolution with computational resources comparable to URANS [24,26]. In the Chimera based parallelization strategy [29], the computational domain is decomposed into a number of zones with five-point overlap as shown in figure 1. In the solution process, each zone is assigned to a separate processor and communication between them is accomplished through the interpolation points in the overlapped region by explicit message passing using MPI libraries. The 3rd order Roe scheme was used for the spatial discretization for both the flow and the turbulent equations.

DETACHED EDDY SIMULATIONS

In the DES formulation, the turbulent kinetic energy dissipation rate (ε) is adjusted in the two-equation k-ε based DES model to enable the transition from the RANS to LES type solution. This is achieved through a limiter that is a function of the local turbulent length scale and the local grid dimension. Accordingly the turbulent kinetic energy dissipation rate in the DES formulation (ε_{DES}) is given below in terms of ε in the original two-equation k-ε turbulence model of Jones and Launder [34]:

$$\frac{\varepsilon_{DES}}{\varepsilon} = F_{DES} * + (1 - F_{DES}) * \left[\max\left(1, \frac{l_{k-\varepsilon}}{C_b * \Delta}\right)\right] \quad (1)$$

In the above equation

$$F_{DES} = AINT\left[\min\left(\frac{C_b * \Delta}{l_{k-\varepsilon}}, 1.0\right)\right] \quad (2)$$

$l_{k-\varepsilon}$ is the turbulent length scale and Δ is defined in terms of the local computational grid Δ_{max} and the convection length scale $\Delta t * \sqrt{u_i^2}$.

$$l_{k-\varepsilon} = \frac{k^{3/2}}{\varepsilon} \quad (3)$$

$$\Delta = \max\left[\Delta_{max}, \Delta t * \sqrt{u_i^2}\right] \quad (4)$$

$$\sqrt{u_i^2} = \sqrt{u^2 + v^2 + w^2} \quad (5)$$

$$\Delta_{max} = \max\,[\Delta x, \Delta y, \Delta z] \quad (6)$$

In Equation 2, AINT is a FORTRAN90 function that truncates the fractional portion of the argument [35] depending on the ratio of the effective grid length

scale $C_b * \Delta$, and the turbulent length scale ($l_{k-\varepsilon}$). In the fine grid regions where, $C_b * \Delta < l_{k-\varepsilon}$, $\varepsilon_{DES} > \varepsilon$ and the eddy viscosity (μ_t) is reduced relative to the original RANS value. Otherwise, in the coarse grid regions where $C_b * \Delta > l_{k-\varepsilon}$, the eddy viscosity remains as predicted by the baseline RANS model [34].

FLOW AND BOUNDARY CONDITIONS

The geometry cavity geometry in the current investigation is similar to the configuration used in the experimental investigation of DERA [36] with and without pulsed injection in a cavity that has a length-to-depth ratio L/D)of 5.0 and a width-to-depth ratio (W/D) of 0.5. The experimental results were obtained at a Reynolds number of 4.336×10^6/ft and a transonic Mach number of 1.19. The present simulations were performed at the same experimental Mach number, but at a Reynolds number of 0.60×10^6/ft, which is $(1/7)^{th}$ the value of the experimental Reynolds number, to optimize the use of available computational resources while maintaining a fully turbulent boundary layer upstream of the cavity front bulkhead. Referring to figure, the length of the plate upstream of the cavity was 4.5D in order to maintain the incoming boundary layer thickness δ at 10% of the cavity depth D as in the experiment. The computational grid consisted of 300×120×80 grid points in the stream-wise, wall normal and span-wise direction respectively, based on prior assessment [24] of the grid resolution influence on SPL spectra and TKE cascading. The grid was packed near the walls, with a minimum wall normal grid spacing of 1×10^{-4}D which corresponds to an y^+ of 1.0 for the first grid point. The grid was clustered in the wall normal direction using hyperbolic tangent stretching function with 20 grid points within the boundary layer upstream of the cavity. More resolution is provided with 35 grid points in the injection region between 4.2D and 4.35D upstream of the cavity as shown in figure 3.

Referring to Fig. 4, free stream conditions were set for the supersonic inflow and first order extrapolation was applied at the upper boundary, which was at 9D above the cavity opening. First order extrapolation was also applied at the downstream boundary, 4.5D behind the rear bulkhead. Periodic boundary conditions were applied in the span-wise direction and no-slip adiabatic boundary conditions were used at the solid walls.

Active flow control was simulated by specifying constant mass flux rates through the injection region for steady blowing; and a velocity profile that is function of space and time for pulsed injection. The unsteady mass injection in the experiment [36] was delivered by a series of powered resonance tubes [12,37] located upstream of the cavity front bulkhead that were fed by a single plenum. Efforts were made to simulate the experiment as closely as possible through proper spatial variation of injection velocity. Two forcing frequencies of 25000 Hz and 5000 Hz were considered, corresponding to the peak frequency obtained from pulsed jets emanating from a resonance tube [33], and the fluctuating injection velocity was always positive. At the plane of the jet exit for both the steady and pulsed injection, the pressure was obtained from the inviscid normal momentum equation [19].

RESULTS AND DISCUSSIONS

Simulations were performed for the baseline cavity flow without injection, for actuated flow with steady mass injection at three blowing ratios, and for two unsteady pulsed mass blowing as listed in Table 1. Parallel computations for twelve overlapping zones in the solution domain were performed using Itanium cluster machines and exclusive message passing with MPI libraries. The DES simulations were initiated in the unsteady mode from an established solution without injection and continued over 100,000 constant time-steps of 4.2345×10^{-7} seconds to obtain sufficient data for statistical analysis. The sound pressure level (SPL) and the turbulent kinetic energy (TKE) spectra for all the simulations were computed based on 65536 sample points. Computational results are presented for the vorticity contours, SPL spectra, grid resolved TKE profiles and the TKE spectra. The SPL spectra are compared with the available experimental data [36] as well as with the LES computational results [19].

Figure 5 present the Mach number contours at the cavity mid-span for the cases listed in table 1. The baseline case without injection shows the formation of a week oblique shock upstream of the cavity. The injection cases show a stronger near normal shock that moves further upstream with increased injection mass flow. This is especially noticeable in the case of steady injection with the thickening of the upstream boundary layer. Zhuang et al. [38] observed experimentally similar shock movement in the case of supersonic cavities with microjets, and Rizzetta et al. [19] reported similar behavior from LES simulations with pulsed injection.

Figure 6 shows the instantaneous contours of the spanwise vorticity component at the cavity mid-span for the baseline and all the controlled cases. One can see the formation of counter rotating vortex in the upstream region with injection, that is more prominent for the unsteady injection simulations with BR=1.2 and f=5,000 Hz. A considerable reduction in the resolved scales within the cavity can be seen in the cases of steady mass injection.

Figure 7 and 8 present the SPL (Sound Pressure Level) spectra for the baseline and the controlled cases, on the cavity floor at X/L = 0.8 and at the cavity rear wall. The computed SPL spectra are compared with the experimental data [36] as well as the LES simulations [19]. The computed SPL spectra for the controlled cases show a greater reduction in the peak SPL amplitude with increased injection ratio. In addition the predicted reduction in the peak SPL is greater for unsteady injection compared to steady mass injection at the same mass ratio. At the maximum simulated steady and unsteady injection mass flow ratios of 0.064 and 0.086 the SPL peak reductions are comparable to the experimental 10-13 dB reduction measured at a higher pulsed mass injection ratio of 0.411.

Figure 9 shows the computed time-mean spanwise averaged grid resolved turbulent kinetic energy plots, and Figure 10 shows the resolved TKE profiles at three streamwise locations. One can see that for the steady injection, there is first an increase then a decrease in the resolved turbulent kinetic energy (TKE) across the cavity opening. On the other hand, unsteady injection reduces the TKE throughout the shear layer across the whole cavity opening. The maximum reduction is observed in the unsteady injection case with BR = 0.9 and f = 25,000 Hz. Several researchers [13, 14] have come up with theories related to the reduction in turbulent kinetic energy at high frequency forcing. According to Wiltse and Glazer [14], the decrease in the turbulent kinetic energy is cause by an accelerated transfer of energy from low frequency to high frequency. On the other hand, according to Stanek et al. [13], this reduction can be attributed to the decreased TKE production due to shear layer stabilization.

Figure 11a presents the computed TKE spectra at one location within the shear layer at the centerline of the cavity opening for the two unsteady injection simulations. The reduction in TKE amplitude with injection can be seen at frequencies below that of the injection forcing. However, pulsed mass injection results in an increased TKE amplitude at and above the actuation frequencies for both $f = 2.5\times10^4$ Hz and $f = 5\times10^3$ Hz. Rizzetta et al. [19] reported similar changes in the TKE spectra with pulsed injection from LES predictions. Figure 11b illustrates the observations made by Stanek et al. [13] in their explanation of high frequency injection effects and substantiates the numerical results presented in Figure 11a.

CONCLUSIONS

The present investigation shows that DES successfully resolves the high-speed unsteady flow and cavity acoustic field including the effects steady and unsteady injections and the physics associated with active control. The presented results indicate that the turbulent kinetic energy level decreases downstream of injection. A reduction of 7–8 dB in peak SPL at the dominant frequency is predicted at steady injection mass ratios of 0.6, 0.9 and 1.2. Unsteady blowing results agree with the experimental results and the LES data, and indicate greater reduction in peak SPL (10-13 dB) than steady injection. The unsteady injection simulations also predict the experimentally observed increase in the turbulent kinetic energy near the actuation frequency.

ACKNOWLEDGEMENTS

The authors would like to thank Dr. Don Rizzetta at AFRL, WPAFB for providing the LES simulation data and the experimental data for the SPL spectra and Dr. Mike Stanek for some helpful suggestions. Majority of the computations were carried out in the Itanium 2 Cluster at the Ohio Supercomputer Center (OSC) and in the AMD Athlon cluster at UC. The authors would like to acknowledge Mr. Robert Ogden of the Aerospace Engineering Department at UC for his technical support.

REFERENCES

1. Franke, M.E., and Sarno, R., “Suppression of Flow Induced Pressure Oscillations in Cavities”, AIAA paper 90-4018, October 1990.
2. Heller, H.H. and Bliss, D.B., “The Physical Mechanism of Flow Induced Pressure Fluctuations in Cavities and Concepts for their Suppression”, AIAA Paper 75-4591, 1975.
3. McGrath, S. and Shaw, L., “Active Control of Shallow Cavity Acoustic Resonance”, AIAA-96-1949, 1996.
4. Stanek, M.J., Ross J.A., Odedra, J., and Peto, J., “High Frequency Acoustic Suppression-The Mystery of the Rod-in-

Crossflow Revealed", AIAA Paper 2003-0007, 2003.
5. Smith, D.L., and Shaw, L.L., "Prediction of the Pressure Oscillations in Cavities Exposed to Aerodynamic Flow, AFFDL-TR-75-34, October 1975.
6. Vakili, A.D., and Gauthier, C., "Control of Cavity Flow by Upstream Mass Injection", Journal of Aircraft, Vol. 31(1), pp 169-174 Jan-Feb 1994.
7. Smith, B.R., Jordan, J.K., Rizk., S.N., Shaw, L., "Computational Simulation of Active Control of Cavity Acoustics", AIAA Paper 2000-1927.
8. Shaw, L., and Northcraft, S., "Closed Loop Active Control for Cavity Acoustics", AIAA Paper 99-1902.
9. Cattafesta III, L.N., Shukla, D., Garg, S., and Ross, J.A., "Development of an Adaptive Weapons-Bay Suppression System", AIAA paper 99-1901.
10. Kegerise, M.A., Cattafesta III, L.N., Ha, C., "Adaptive identification and Control of Flow-Induced Cavity Oscillations", AIAA Paper 2002-3158.
11. Kastner, J., and Samimy, M., "Effects of Forcing Frequency on the Control of an Impinging High Speed Jet", AIAA Paper 2003-0006 2003.
12. Stanek, M.J., Raman, G., Kibens, V., Ross, J.A., Odedra, J, Peto, J.W., "Control of Cavity Resonance Through Very High Frequency Forcing", AIAA Paper 2000-1905.
13. Stanek, M.J., Raman, G., Ross, J.A., Odedra, J, Peto, J.W., Alvi, F., Kibens, V, "High frequency acoustic suppression-The Role of Mass Flow, The notion of Superposition, and The Role of Inviscid Instability-A New Model (Part-II), AIAA Paper 2002-2404, 2002.
14. Wiltse, J.M., and Glezer, A., "Direct Excitation of Small Scale Motions in Free Shear Flows", Physics of Fluids, Vol. 10(8), pp 2026-2036, 1998.
15. Ukeiley, L.S., Ponton, M.K., Seiner, J.M., and Jansen, B., "Suppression of Pressure Loads in Resonating Cavities Through Blowing", AIAA Paper 2003-0181, 2003.
16. Zhuang, N., Alvi, F.S., Alkislar, M.B., Shih, C., Sahoo, S., and Annaswamy, A.M., "Aeroacoustic Properties of Supersonic Cavity Flows and Their Control", AIAA Paper 2003-3101.
17. Bortz, D.M., Rubio, A.D., Banks, H.T., Cain, A.B., Smith, R.C., "Control of Open Bay Acoustics by Harmonic Mass Injection", International Journal of Aeroacoustics, Vol. 1(1), pp 65-81, 2002.
18. Cain, A.B., Rubio, A.D., Bortz, D.M., Banks, H.T., Smith, R.C., "Optimizing Control of Open Bay Acoustics", AIAA Paper 2000-1928, 2000.
19. Rizzetta, D.P. and Visbal, M.R., "Large Eddy Simulation of Supersonic Cavity Flowfields Including Flow Control", AIAA Paper 2002-2853, 2002.
20. Arunajatesan, S., Shipman, J, D., and Sinha, N., "Hybrid RANS-LES Simulation of Cavity Flow Fields with Control", AIAA Paper 2002-1130, 2002.
21. Arunajatesan, S., Shipman, J, D., and Sinha, N., Seiner, J.M., "Mechanisms in High-Frequency Control of Cavity Flows", AIAA Paper 2003-0005, 2003.
22. Hamed, A., Basu, D., Mohamed, A. and Das, K. "Direct Numerical Simulations of High Speed Flow over Cavity," Proceedings (TAICDL), August 5-9, 2001, Arlington, Texas.
23. Hamed, A., Basu, D., and Das, K., "Effect of Reynolds Number on the Unsteady Flow and Acoustic Fields of a Supersonic Cavity," ASMEFEDSM2003-45473, 2003.
24. Hamed, A., Basu, D., and Das, K., "Assessment of Hybrid Turbulence Models for Unsteady High Speed Separated Flow Predictions", AIAA Paper 2004-0684, 2004.
25. Hamed, A., Basu, D., and Das, K., "Numerical Simulations of Fluidic Control for Transonic Cavity Flows", AIAA Paper 2004-0429, 2004.
26. Das, K., Hamed, A. & Basu, D., "Numerical Investigations Of Transonic Cavity Flow Control Using Steady And Pulsed Fluidic Injection", FEDSM2005-77422, ASME FEDSM, Houston, TX, Jun 19-23, 2005.
27. Beam, R., and Warming, R., "An Implicit Factored Scheme for the Compressible Navier-Stokes Equations," 1978, AIAA Journal, Vol. 16, No. 4, pp. 393-402.
28. Gaitonde, D., and Visbal, M. R., "High-Order Schemes for Navier-Stokes Equations: Algorithm and Implementation into FL3DI", 1998, AFRL-VA-TR-1998-3060.
29. Morgan, P., Visbal, M., and Rizzetta, D., "A Parallel High-Order Flow Solver for LES and DNS", 2002, AIAA-2002-3123.
30. Visbal, M. R. and Gaitonde, D., "Direct Numerical Simulation of a Forced

Transitional Plane Wall Jet", 1998, AIAA 98-2643.
31. Basu, D., Hamed, A., and Das, K., "DES and Hybrid RANS/LES models for unsteady separated turbulent flow predictions", 2005, AIAA-2005-0503.
32. Basu, D., Hamed, A., and Das, K., "Comparative Analysis of Hybrid Turbulence Closure Models in the Unsteady Transonic Separated Flow Simulations", 2006, 44th AIAA Aerospace Sciences Meeting and Exhibit, Reno, Nevada, AIAA - 2006-0117.
33. Basu, D., Hamed, A., and Das, K., "DES, Hybrid RANS/LES and PANS models for unsteady separated turbulent flow simulations", 2005, Proceedings of FEDSM'05, Houston, 19-23 June, 2005, FEDSM-2005-77421.
34. Jones, W. P., and Launder, B. E., "The prediction of laminarization with a two-equation model of turbulence", 1972, International Journal of Heat and Mass Transfer, Vol. 15, pp. 301-313.
35. Baurle, R. A., Tam, C. J., Edwards, J. R., and Hassan, H. A., "Hybrid Simulation Approach for Cavity Flows: Blending, Algorithm, and Boundary Treatment Issues", 2003, AIAA Journal, Vol. 41, No. 8, pp. 1463-1480.
36. Ross, J.A., Odedra, J., and Peto, J, 1998, DERA Bedford Internal Report, MSSA CR980744/1.0.
37. Hamed. A., Das, K., Basu, D., "Numerical Simulation and Parametric Study of Hartmann-Sprenger Tube Based Powered Device," AIAA Paper 2003-0550, 2003.
38. Zhuang, N., Alvi, F.S., Alkislar, M.B., Shih, C., Sahoo, S., and Annaswamy, A.M., "Aeroacoustic Properties of Supersonic Cavity Flows and Their Control", AIAA Paper 2003-3101.

Table 1. Simulated and Experimental injection mass flow rates

Conditions	Re / feet	Injection ratio (BR) = $\frac{\dot{m}_{injection}}{\dot{m}_{boundarylayer}}$	Actual mass injection rate (lbm/sec)
Baseline (no injection)	0.60×10^6	0.0	0.0
Steady injection	0.60×10^6	0.6	0.043
Steady injection	0.60×10^6	0.9	0.064
Steady injection	0.60×10^6	1.2	0.086
Unsteady injection f = 25,000 Hz	0.60×10^6	0.9	0.064
Unsteady injection f = 5,000 Hz	0.60×10^6	1.2	0.086
Experiment Ref. [36] f=5,000 Hz	4.33×10^6		0.411
LES Ref. [19] f=5,000 Hz	0.12×10^6	1.41	0.5

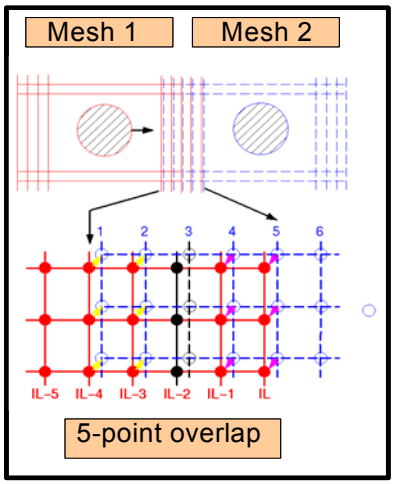

Figure 1 Schematic of the domain connectivity and five-point overlap for the parallel solver

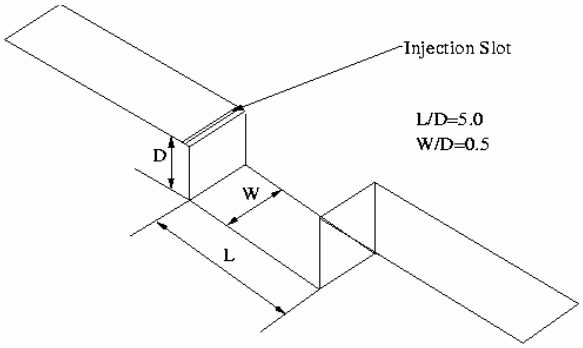

Figure 2 Schematic of the computational domain with injection slot

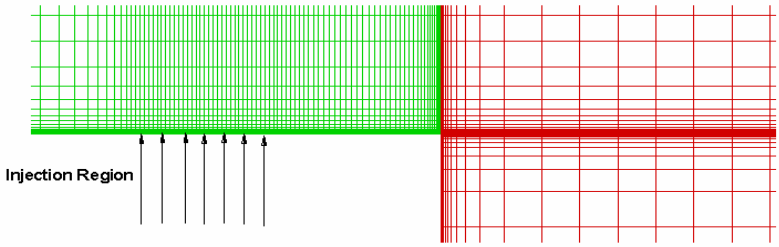

Figure 3 Computational grids showing the injection region

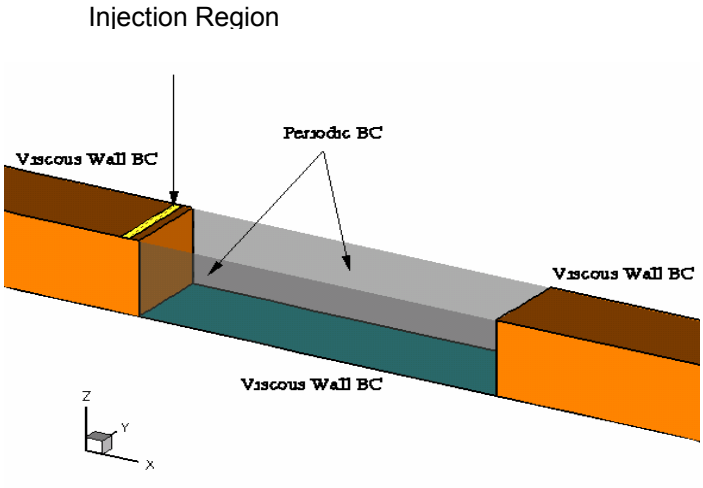

Figure 4 Schematic of boundary conditions

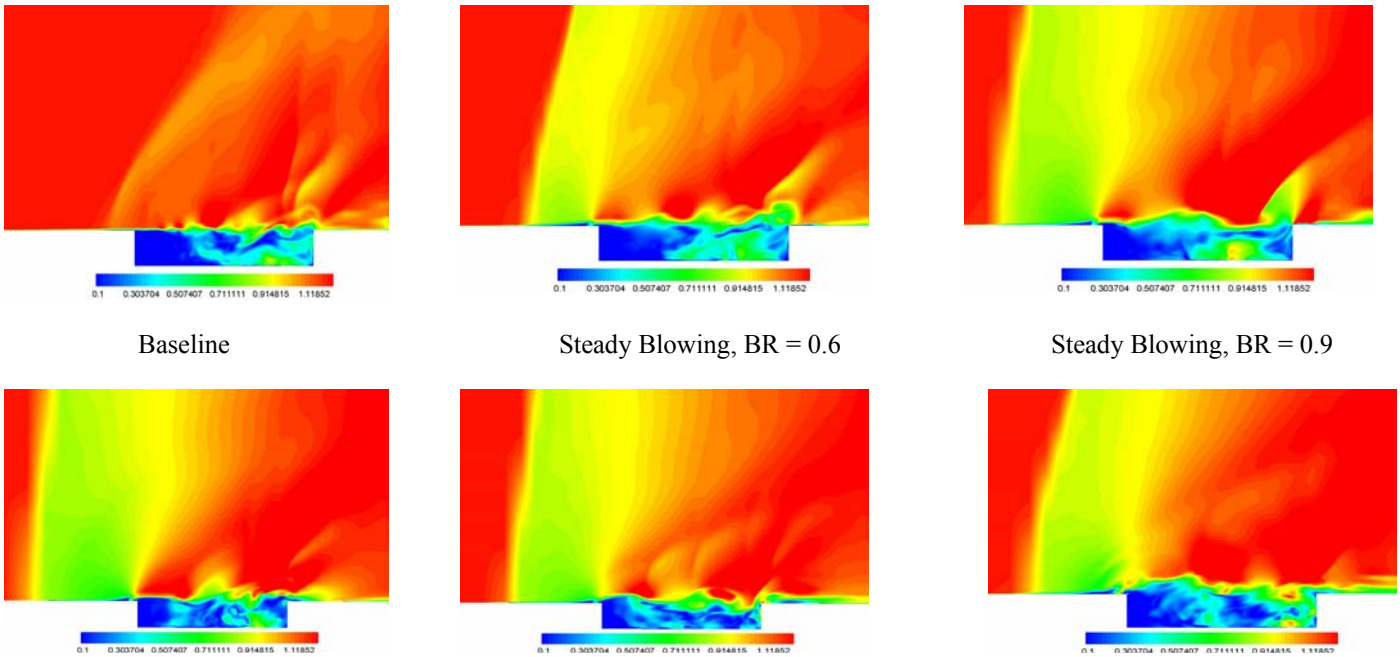

Figure 5 Cavity mid-span Mach number contours for different blowing ratios

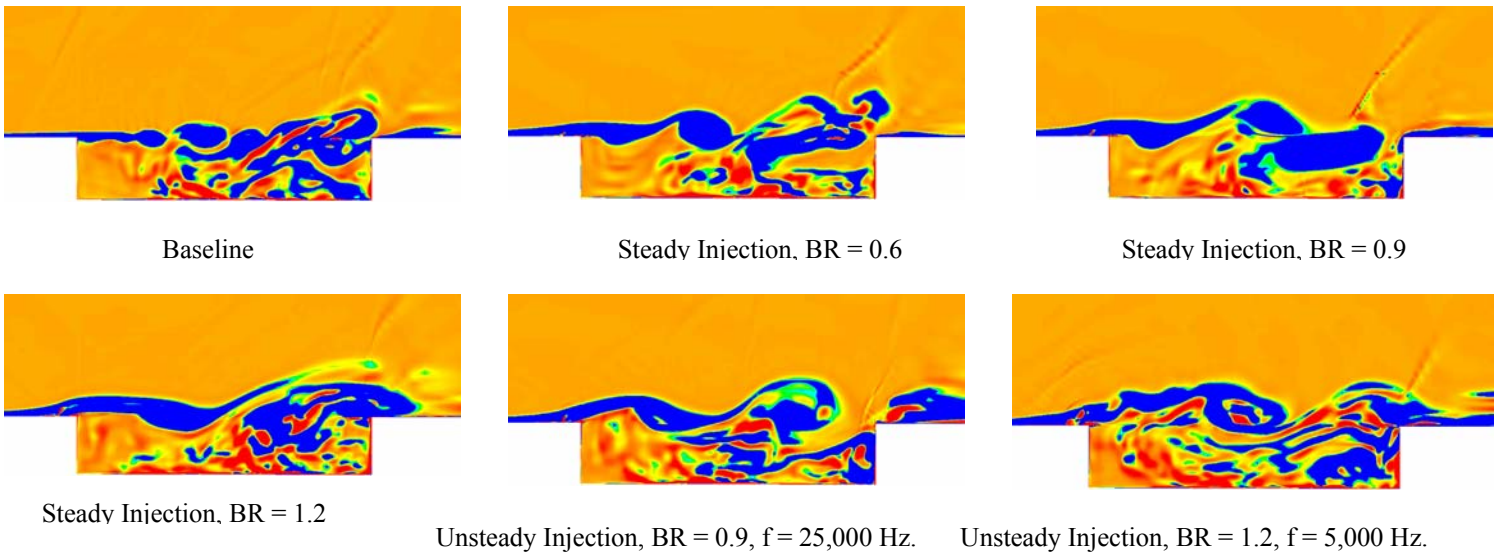

Figure 6 Contours of spanwise vorticity component at cavity mid-span

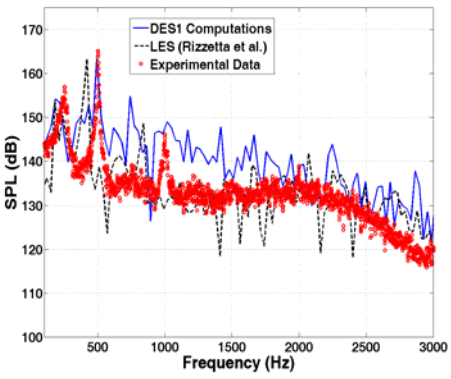

Baseline

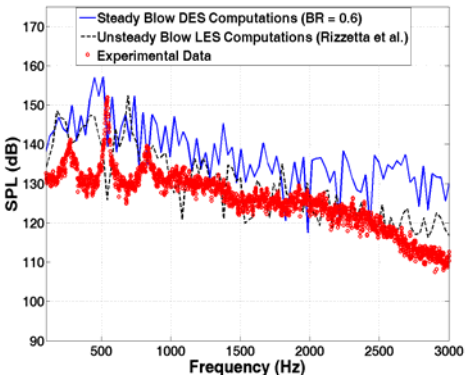

Steady Injection, BR = 0.6

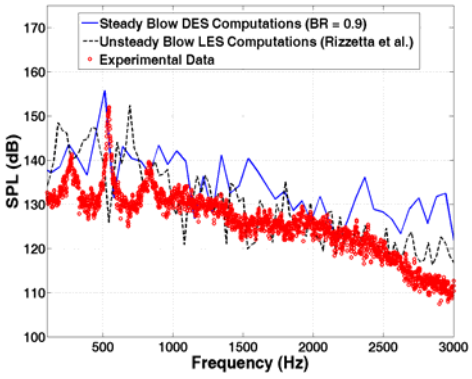

Steady Injection, BR = 0.9

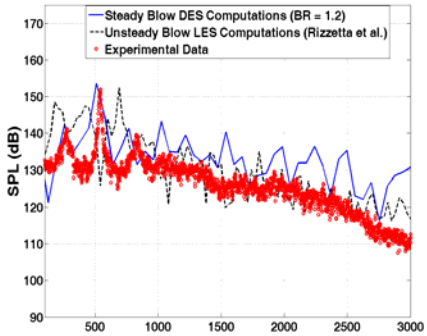

Steady Injection, BR = 1.2

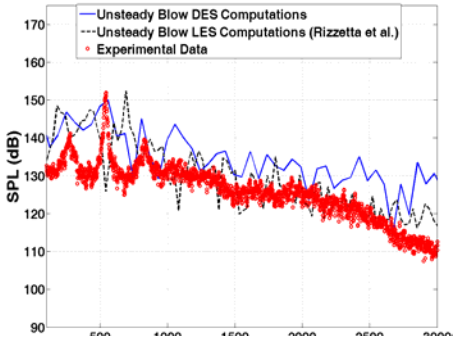

Unsteady Injection, BR = 0.9, f = 25,000 Hz.

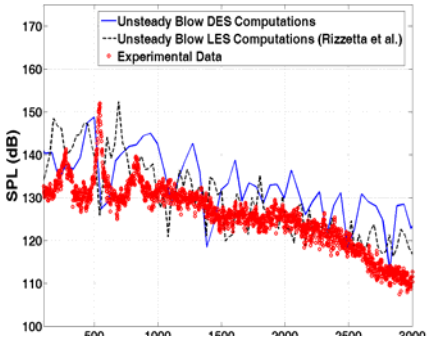

Unsteady Injection, BR = 1.2, f = 5,000 Hz.

Figure 7 Spanwise averaged SPL spectra on the cavity floor (X/L = 0.8, Y/D = 0.0)

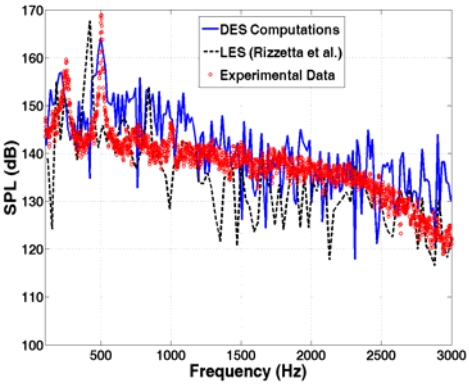

Baseline

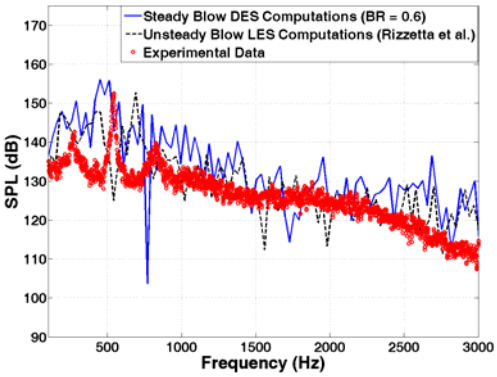

Steady Injection, BR = 0.6

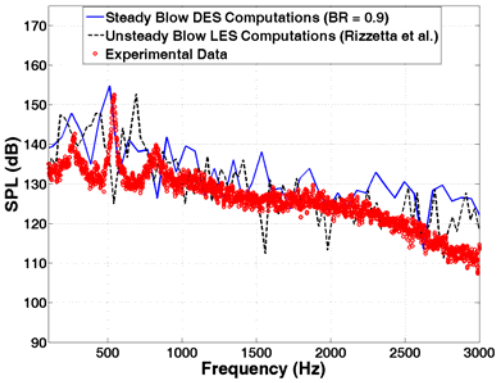

Steady Injection, BR = 0.9

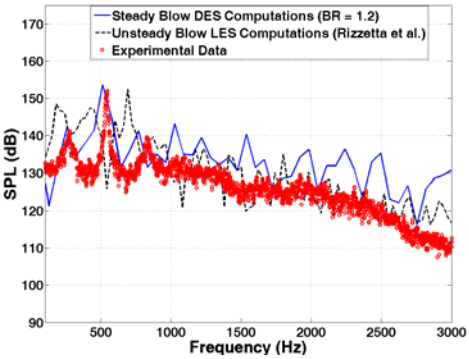

Steady Injection, BR = 1.2

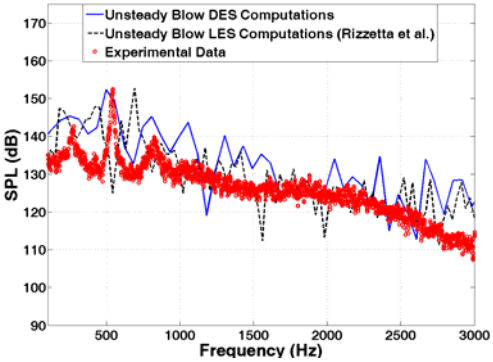

Unsteady Injection, BR = 0.9, f = 25,000 Hz.

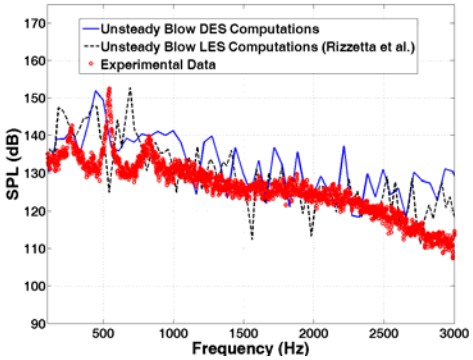

Unsteady Injection, BR = 1.2, f = 5,000 Hz.

Figure 8 Spanwise averaged SPL spectra on the cavity rear wall (X/L = 1.0, Y/D = 0.5)

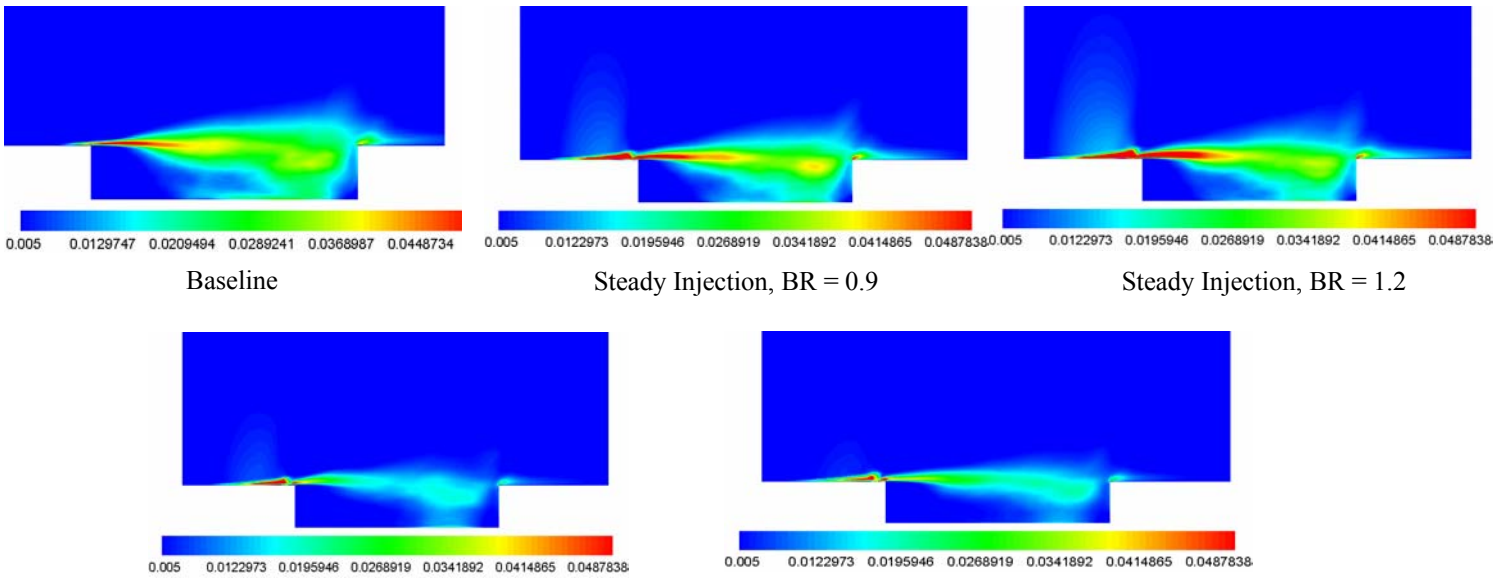

Baseline | Steady Injection, BR = 0.9 | Steady Injection, BR = 1.2

Unsteady Injection, BR = 0.9, f = 25,000 Hz. | Unsteady Injection, BR = 1.2, f = 5,000 Hz.

Figure 9 Time-mean spanwise averaged resolved turbulent kinetic energy (TKE) contours

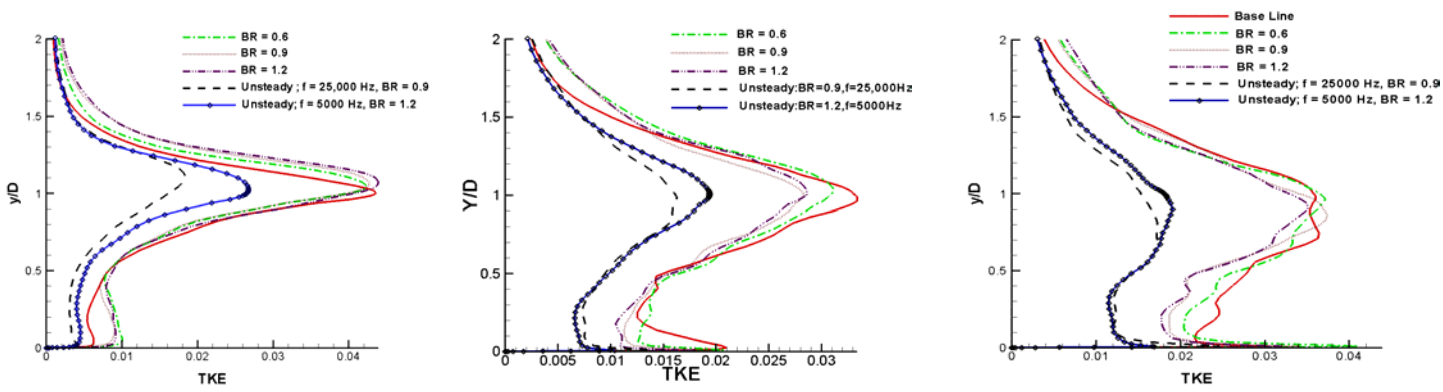

X/L = 0.2 | X/L = 0.5 | X/L = 0.8

Figure 10 Time-mean spanwise averaged grid resolved turbulent kinetic energy profiles across cavity shear layer

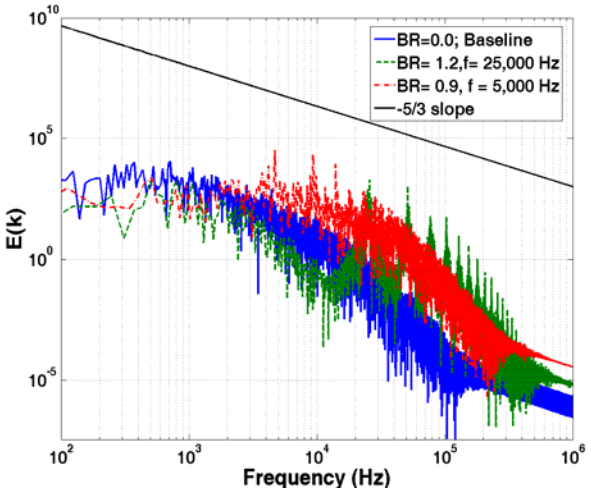

Figure 11a Resolved Turbulent Kinetic Energy (TKE) spectra in cavity shear layer for unsteady injection (X/L = 0.2, Y/D = 1.0)

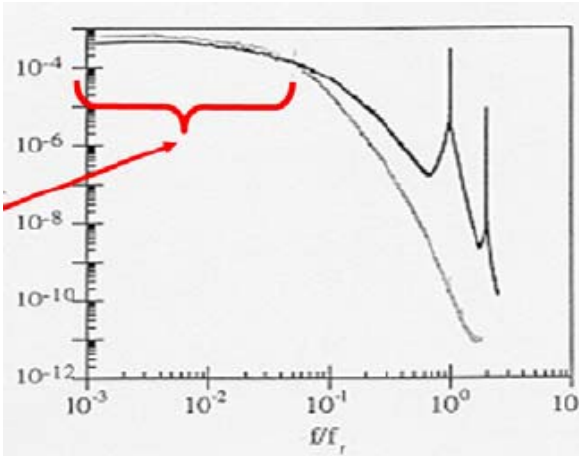

Figure 11b High Frequency Forcing Observations by Stanek et al. [13]